

Supplementary Information

Origin of high piezoelectricity of inorganic halide perovskite thin films and their electromechanical energy-harvesting and physiological current-sensing characteristics

Da Bin Kim, Kwan Hyun Park and Yong Soo Cho*

Department of Materials Science and Engineering, Yonsei University, Seoul 03722, Korea

*Corresponding author: ycho@yonsei.ac.kr (Y.S.Cho)

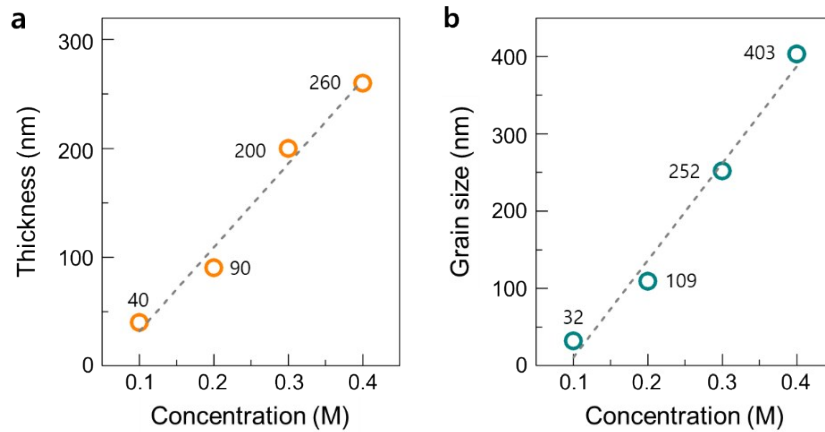


Fig. S1 Variations of (a) thickness and (b) grain size in the annealed CsPbBr₃ thin films processed with different precursor concentration up to 0.4 M.

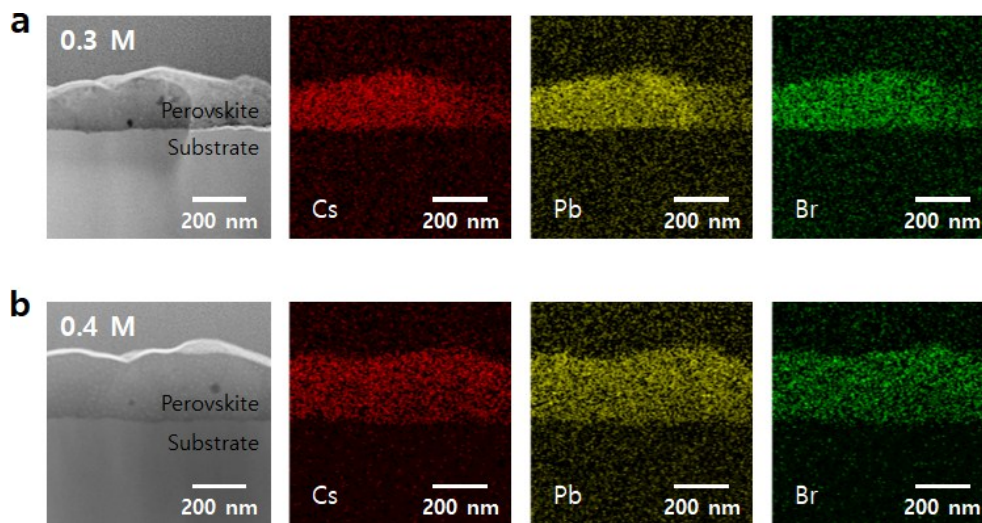


Fig. S2 Cross-sectional scanning transmission electron microscopy (STEM) images and energy-dispersive X-ray spectroscopy (EDS) element-mapping images of the CsPbBr₃ thin films processed with the precursor concentration of (a) 0.3 M and (b) 0.4 M. The mapping images suggest the homogeneous distributions of cesium (in red), lead (in yellow) and bromine (in green) over the cross-section. A scanning transmission electron microscope (Cs-STEM, JEM-ARM200F, JEOL, Japan) operated at 80 kV was used for the observation.

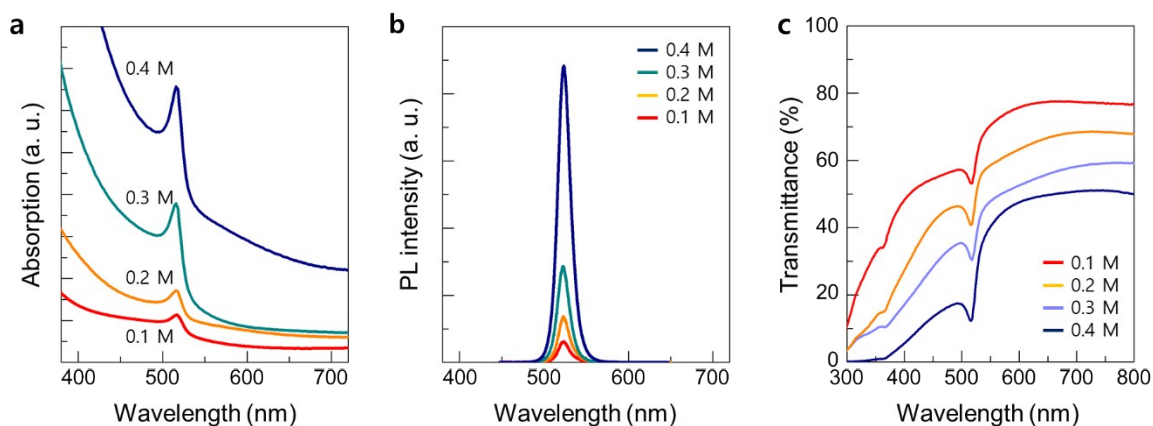


Fig. S3 (a) absorption spectra, (b) photoluminescence spectra, and (c) optical transmittance (%) of the annealed CsPbBr₃ thin films processed with different precursor concentration.

Table S1 Actual values of lattice constants, ratio of b/a , and unit cell volume for different poling fields up to 24.9 kV/cm in the annealed 0.4 M CsPbBr₃ thin films.

Poling field (kV/cm)	Lattice constant (Å)			b/a	Volume (Å ³)
	a	b	c		
0	8.241	11.59	8.246	1.406	787.3
6.2	8.244	11.60	8.269	1.407	790.5
12.4	8.240	11.62	8.262	1.410	790.8
18.7	8.232	11.63	8.241	1.413	789.0
24.9	8.241	11.66	8.269	1.415	794.5

Table S2 Poling field-dependent changes in bonding angles of Pb-Br-Pb in the ac -plane and Br-Pb-Pb and Pb-Br-Pb along the b -axis in the CsPbBr₃ thin films, which were estimated by the VESTA software.

Poling field (kV/cm)	ac-plane	b-axis	
	Pb-Br-Pb (°)	Br-Pb-Pb (°)	Pb-Br-Pb (°)
0	156.699	83.762	164.24
6.2	156.700	83.770	164.25
12.4	156.716	83.783	164.28
18.7	156.726	83.792	164.31
24.9	156.730	83.804	164.33

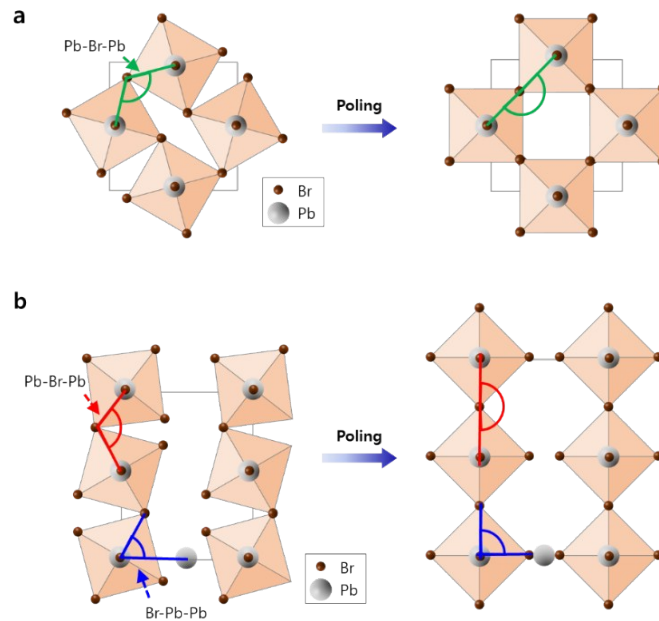


Fig. S4 Schematic illustrations of the ideal alignments of Pb-centered Br₆ octahedra with the perfect poling: (a) top view with the change of the Pb-Br-Pb bonding angle in the *ac*-plane and (b) side view with the changes of the Pb-Br-Pb and Br-Pb-Pb bonding angles along the *b*-axis.

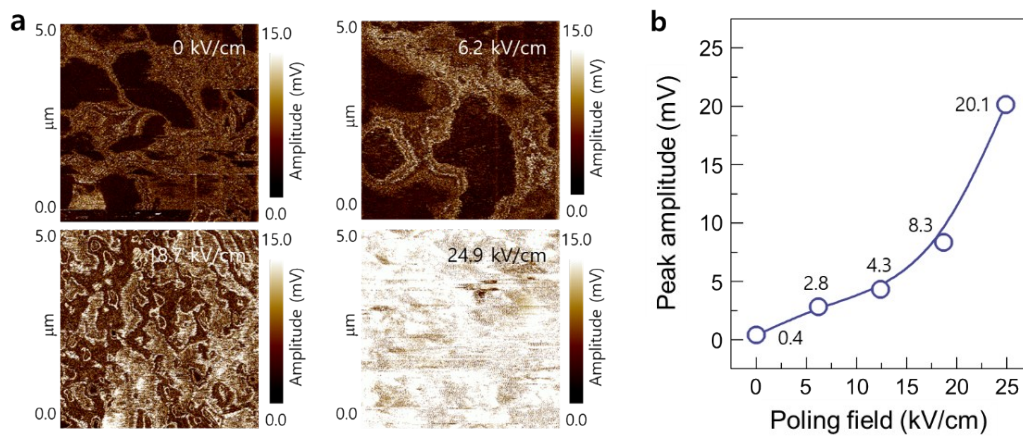


Fig. S5 (a) PFM amplitude images of the CsPbBr₃ thin films poled at different electric fields and (b) the variation in peak amplitude with increasing the poling field.

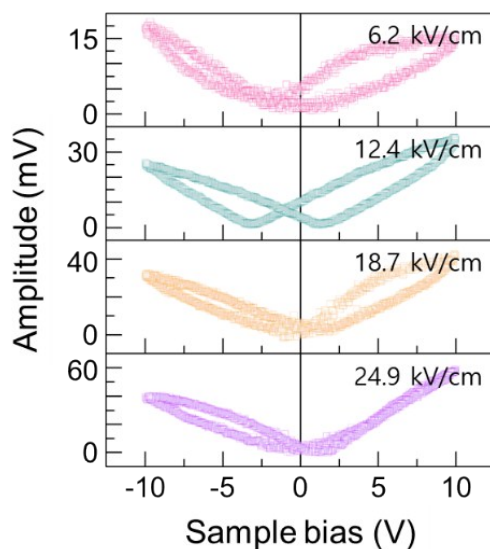


Fig. S6 Butterfly loops of the amplitude-voltage curves for the films poled at different electric fields, which were measured by piezoelectric force microscopy.

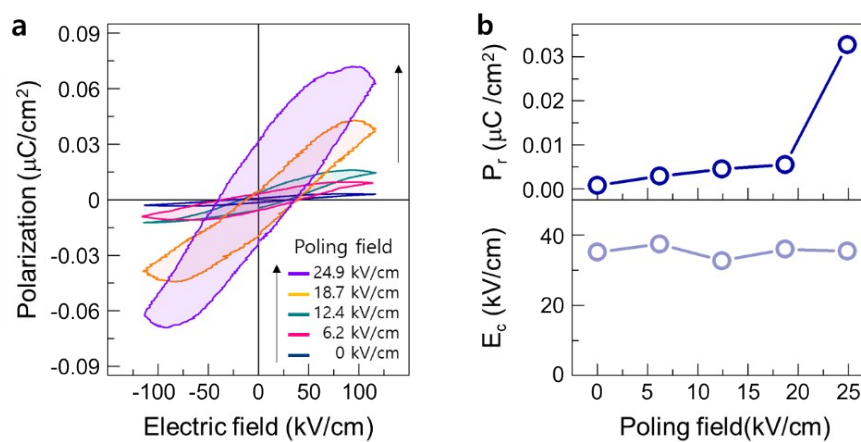


Fig. S7 (a) Polarization-electric field (P-E) hysteresis loop curves (at 50 Hz) of the 0.4 M CsPbBr₃ thin films poled at different electric field and (b) variations of remnant polarization P_r and coercive field E_c with increasing the poling field up to 24.9 kV/cm. (Note that the saturation polarization was not presented because some curves did not seem to be fully saturated)

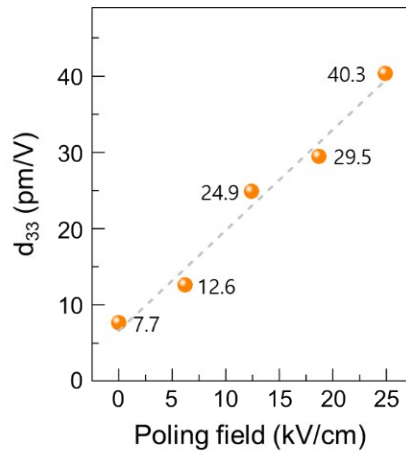


Fig. S8 Effective piezoelectric coefficient, $d_{33,\text{eff}}$ for the annealed CsPbBr₃ thin films poled at different electric fields up to 24.9 kV/cm, which were estimated from the PFM measurements.

Table S3 Effective piezoelectric coefficients reported for halides-based perovskite materials in different types of sample, e.g., thin film and single crystal.

Ref.	Materials	Type of materials	$d_{33,\text{eff}}$ (pm/V)
this work	CsPbBr ₃	Thin film	7.7 (unpoled)
			40.3 (poled)
1	MAPbI ₃	Thin film	6
2	MAPbI ₃	Thin film	4.2
3	MAPbI ₃	Thin film	5.12
4	MASnI ₃	Thin film	20.8
5	FAPbBr ₃	Thin film	25
6	MAPbI ₃	Single crystal	2.7
7	MAPbI ₃	Single crystal	3.1



Fig. S9 A photograph of the CsPbBr₃ thin film-based energy harvester.

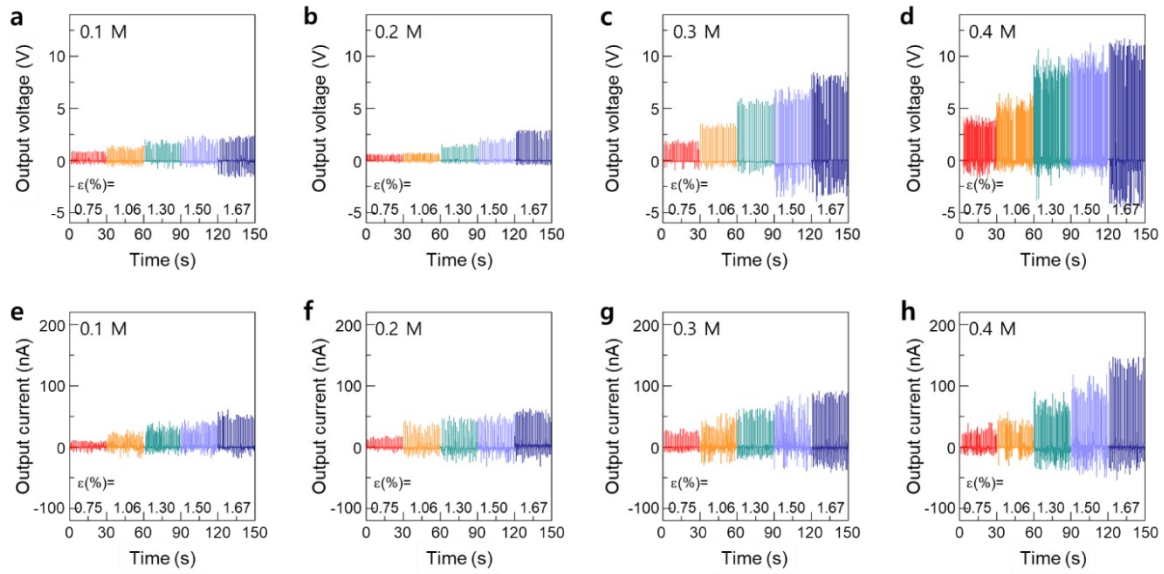


Fig. S10 (a-d) output voltage and (e-f) output current generated at 1 Hz with repetitive bending operations for the CsPbBr₃ thin film-based energy harvesters, which are dependent on the precursor concentration of 0.1 to 0.4 M and the bending strain of 0 to 1.67 %.

Table S4 Calculated bending strain applied to the flexible CsPbBr₃ energy harvesters, which were estimated with the bending (radius) curvature determined by the change in sample length (ΔL).

ΔL (mm)	Radius (mm)	Applied strain (%)
5	11.70	0.75
10	8.27	1.06
15	6.75	1.30
20	5.75	1.50
25	5.23	1.67

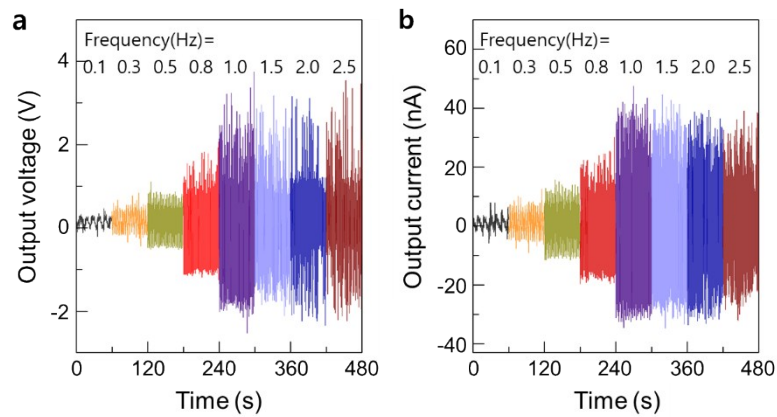


Fig. S11 Bending frequency-dependent (a) output voltage and (b) output current of the unpoled 0.1 M CsPbBr₃ energy harvesters.

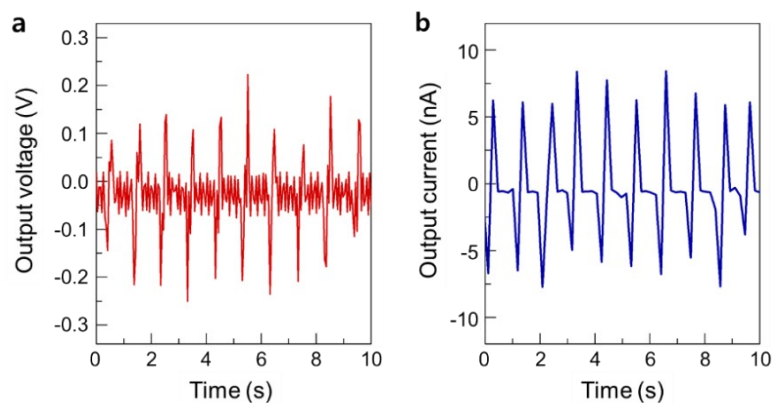


Fig. S12 (a) Output voltage and (b) output current generated for the PET/ITO/PDMS/ITO/PET sample (without the CsPbBr₃ layer).

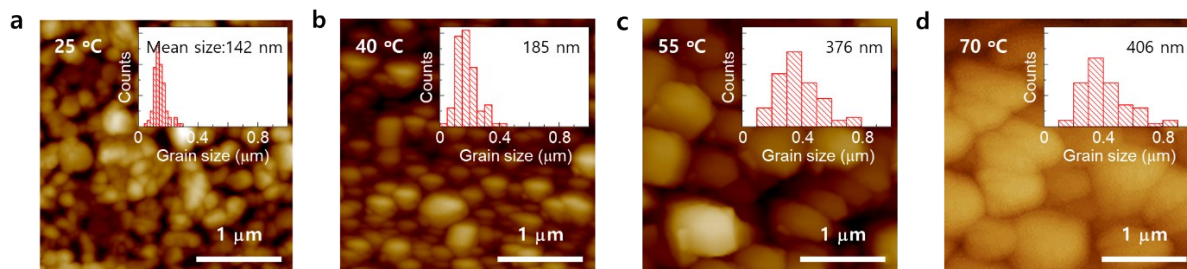


Fig. S13 AFM images of surface morphology (3 μm x 3 μm) of the perovskite thin films prepared at different annealing temperatures of (a) 25 $^{\circ}\text{C}$, (b) 40 $^{\circ}\text{C}$, (c) 55 $^{\circ}\text{C}$, and (d) 70 $^{\circ}\text{C}$, which demonstrate the increase of grain size with the higher annealing temperature. The inset shows the grain size distribution of each film with average grain size.

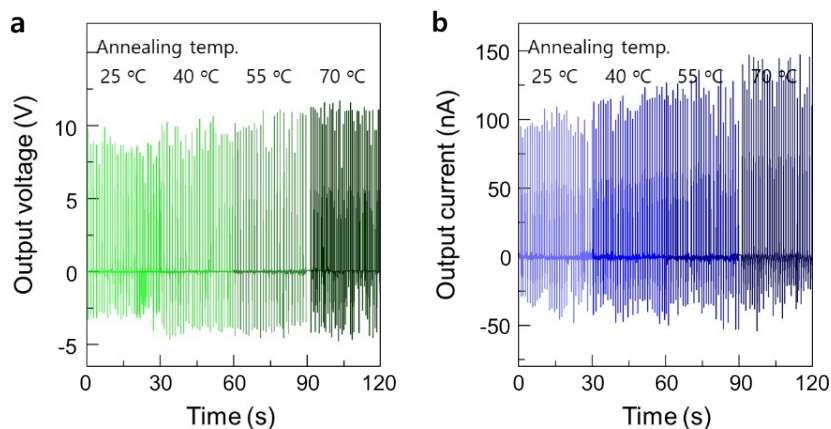


Fig. S14 Piezoelectric energy harvesting performance of (a) output voltage and (b) output current for the 0.4 M CsPbBr₃ harvesters prepared at different annealing temperatures from 25 to 70 $^{\circ}\text{C}$. The energy harvesters were periodically bent with a strain of 1.67% at the bending frequency of 1 Hz.

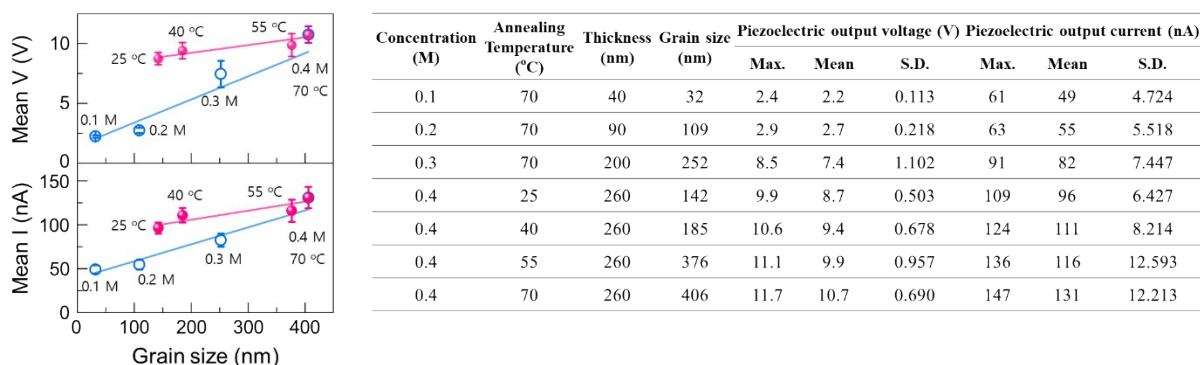


Fig. S15 Dependence of output voltage and current with the variations in grain size (which were obtained by different precursor concentration and annealing temperature): the pink line indicates the grain size dependence when the film thickness is identical whereas the blue line corresponds to the combined effects of grain size and film thickness (thus the dependency becomes large). All the corresponding maximum, mean, and standard deviation of peak values are listed in the right-side table, with the experimental condition used to figure out the grain size effect.

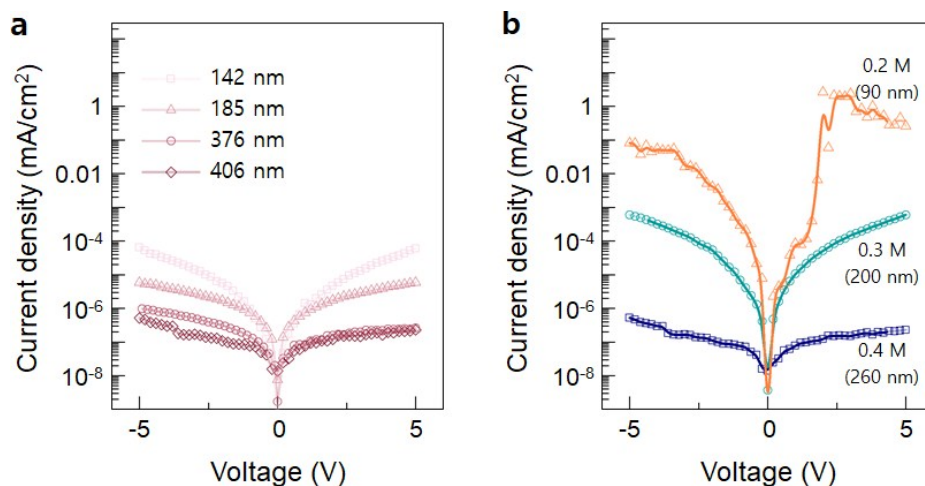


Fig. S16 Current density-voltage curves of the CsPbBr₃ thin films processed with (a) different grain sizes of 142 nm to 406 nm for the fixed film thickness of 260 nm and (b) different precursor concentrations of 0.2 M to 0.4 M. Note that the different precursor concentration also changes the film thickness as well as the grain size.

Table S5. Performance comparisons in halide perovskites-based piezoelectric energy harvesters.

Ref.	Materials	Material type	Dimension (cm ²)	Poling condition	Output voltage (V)	Output current (nA)
This work	CsPbBr ₃	Thin film	5	unpoled	11.7	147
				24.9 kV/cm	16.4	604
3	MAPbI ₃	Thin film	1	unpoled	1	50
				80 kV/cm	2.7	140
4	MASnI ₃	Thin film	1	-	3.8	350
5	FAPbBr ₃	Composite (PDMS)	1	unpoled	4	-
				50 kV/cm	8.5	3800
6	MAPbI ₃	Single crystal		-	0.07	-
8	MAPbBr ₃	Composite (PVDF)	3.6	-	5	60
9	MAPbI ₃	Composite (PVDF)	-	-	1.8	37.5
10	MAPb _{1-x} Fe _x I ₃	Thin film	1	unpoled	4.52	500
				30 kV/cm	7.29	880
11	MAPbI ₃	Thin film	0.16	-	0.5	1
12	MAPbBr ₃	Composite (PVDF)	4	-	0.5	-

- [1] M. Coll, A. Gomez, E. Mas-Marza, O. Almora, G. Garcia-Belmonte, M. Campoy-Quiles and J. Bisquert, *J. Phys. Chem. Lett.*, 2015, **6**, 1408-1413.
- [2] J. Song, Z. Xiao, B. Chen, S. Prockish, X. Chen, A. Rajapitamahuni and X. Hong, *ACS Appl. Mater. Interfaces*, 2018, **10**, 19218-19225.
- [3] Y. J. Kim, T. V. Dang, H. J. Choi, B. J. Park, J. H. Eom, H. A. Song and S. G. Yoon, *J. Mater. Chem. A*, 2016, **4**, 756-763.
- [4] S. Ippili, V. Jella, J. H. Eom, J. Kim, S. Hong, J. S. Choi and S. G. Yoon, *Nano Energy*, 2019, **57**, 911-923.
- [5] R. Ding, H. Liu, X. Zhang, J. Xiao, R. Kishor, H. Sun and J. Chen, *Adv. Funct. Mater.*, 2016, **26**, 7708-7716.
- [6] Q. Dong, J. Song, Y. Fang, Y. Shao, S. Ducharme and J. Huang, *Adv. Mater.*, 2016, **28**, 2816-2821.
- [7] B. Chen, T. Li, Q. Dong, E. Mosconi, J. Song, Z. Chen and F. D. Angelis, *Nat. Mater.*, 2018, **17**, 1020-1026.
- [8] A. Sultana, M. M. Alam, P. Sadhukhan, U. K. Ghorai, S. Das, T. R. Middy and D. Mandal, *Nano Energy*, 2018, **49**, 380-392.
- [9] A. Sultana, P. Sadhukhan, M. M. Alam, S. Das, T. R. Middy and D. Mandal, *ACS Appl. Mater. Interfaces*, 2018, **10**, 4121-4130.
- [10] S. Ippili, V. Jella, J. Kim, S. Hong and S. G. Yoon, *Nano Energy*, 2018, **49**, 247-256.
- [11] J. H. Eom, H. J. Choi, S. V. N. Pammi, V. D. Tran, Y. J. Kim, H. J. Kim and S. G. Yoon, *J. Mater. Chem. C*, 2018, **6**, 2786-2792.
- [12] S. Huang, G. Tang, H. Huang, X. G. Wu, P. Zhou, L. Zou and J. Hong, *Sci. Bull.*, 2018, **63**, 1254-1259.

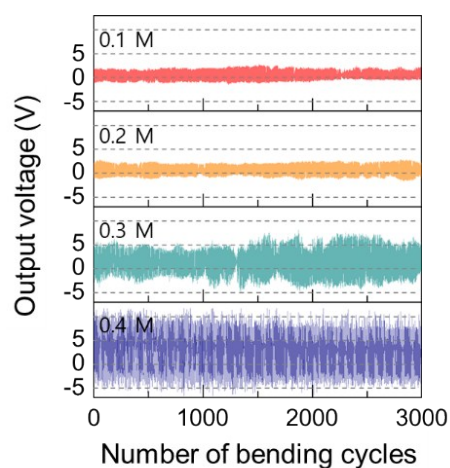


Fig. S17. Variations in output voltage with repetitive bending cycles up to 3,000 times for the unpoled CsPbBr₃ thin films processed with different precursor concentrations.

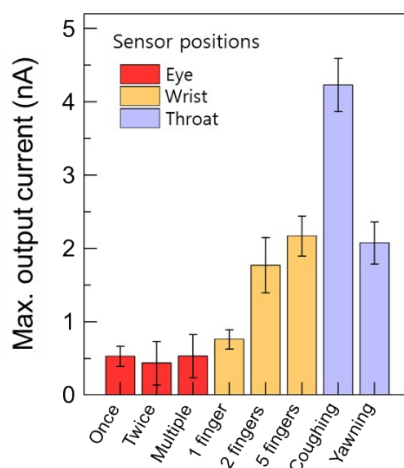


Fig. S18. Bar chart of maximum output current measured by diverse motions, such as eye-blinking, finger-bending, coughing, and yawning, for the patch-type energy harvesters attached to eye, wrist and throat. Mean values of each motion were obtained from the multi-measurement results by five participants. Error bars indicate the 95%-confidence interval.